

Electronic Supplementary Information (ESI)

Ba₂Ge₂Te₅: a ternary NLO-active telluride with unusual one-dimensional helical chains and giant second-harmonic-generation tensors

Mao-Yin Ran,^{‡a,d} Zuju Ma,^{‡b} Xin-Tao Wu,^{a,c,d} Hua Lin,^{*,a,c,d} and Qi-Long Zhu^{*,a,c,d}

^aState Key Laboratory of Structural Chemistry, Fujian Institute of Research on the Structure of Matter, Chinese Academy of Sciences, Fuzhou 350002, China

^bSchool of Environmental and Materials Engineering, Yantai University, Yantai 264005, China

^cFujian Science & Technology Innovation Laboratory for Optoelectronic Information of China, Fuzhou, Fujian 350108, China

^dUniversity of Chinese Academy of Sciences, Beijing 100049, China

[‡]M. Y. Ran and Z. Ma contributed equally to this work.

**E-mail: linhua@fjirsm.ac.cn and qlzhu@fjirsm.ac.cn.*

Electronic Supplementary Information Index

1. Experimental Section

1.1 Materials and Instruments

1.2 Synthesis

1.3 Second-Harmonic Generation (SHG) Measurements

1.4 Single-Crystal Structure Characterizations

2. Computational Details

3. Figures and Tables

Figure S1. The ethane-like [Ge₂Te₆] unit with different conformations in the Ge-

Electronic Supplementary Information (ESI)

based tellurides. For better expression, Te atoms on the [GeTe₃] unit are represented by different colors.

Figure S2. Energy dispersive X-ray (EDX) result and the obtained composition of Ba₂Ge₂Te₅.

Figure S3. Electron localization function (ELF) of Ba₂Ge₂Te₅. Black atoms, Ba; Blue atoms, Ge; Yellow atoms, Te.

Figure S4. X-ray photoelectron spectra (XPS) of (a) Ba, (b) Ge, (c) Te, and (d) survey spectrum for Ba₂Ge₂Te₅.

Figure S5. Powder XRD patterns of Ba₂Ge₂Te₅ heated at 1023K (red) and the simulated one (black).

Figure S6. Cyclic DSC diagrams of Ba₂Ge₂Te₅ between room temperature and 873 K.

Figure S7. Vis-NIR optical absorption spectra of polycrystalline sample Ba₂Ge₂Te₅ at room temperature. The curve of Ba₂Ge₂Te₅ shows a clear absorption edge at 1174 nm, indicating a narrow band gap of about 1.15 eV.

Figure S8. The photograph of single-crystal Ba₂Ge₂Te₅.

Figure S9. The first Brillouin zone with high symmetry points of Ba₂Ge₂Te₅.

Table S1 Crystallographic data and refinement details for Ba₂Ge₂Te₅.

Table S2 Atomic coordinates and equivalent isotropic displacement parameters of Ba₂Ge₂Te₅.

Table S3 Selected bond lengths (Å) and angle (°) of Ba₂Ge₂Te₅.

4. References

1. Experimental Section

1.1 Materials and Instruments

All reagents used in the present experiments were purchased from commercial sources and directly used without further purification. All weighing processes were completed in an anhydrous and oxygen-free glove box. The semi-quantitative energy dispersive X-ray (EDX, Oxford INCA) spectra were measured with a field emission scanning electron microscope (FESEM, JSM6700F). Powder X-ray diffraction (PXRD) analysis was carried out in a Rigaku Mini-Flex II powder diffractometer (Cu-K α , $\lambda = 1.5418 \text{ \AA}$). X-ray photoelectron spectroscopy (XPS) with monochromatized Al K α X-rays ($h\nu = 1486.6 \text{ eV}$) radiation (ThermoFisher Scientific Co. ESCALAB 250, USA) was used to investigate the surface properties. UV-vis-NIR absorption measurement was performed in the region of 200–2500 nm at room temperature using an UV-vis-NIR spectrometer (Perkin-Elmer Lambda 950). The reflectance spectrum of the BaSO₄ powder was collected as the baseline and the diffuse reflectance data were converted to absorbance internally by the instrument by use of the Kubelka-Munk function.¹ The IR transmittance was measured on the PerkinElmer Spectrum One FT-IR Spectrometer in the range of 400–4000 cm⁻¹. The thermal stability analyses were measured on a NETZSCH STA 449C simultaneous analyser.

1.2 Synthesis

Ba (2 N), Ge (5 N), and Te (5 N) were directly purchased from Alfa-Aesar. All manipulations were performed in an Ar-filled glovebox with H₂O and O₂ contents of less than 0.1 ppm. Polycrystalline sample of Ba₂Ge₂Te₅ was obtained by traditional

Electronic Supplementary Information (ESI)

solid-state reactions in a stoichiometric mixture of Ba (0.1374 g, 0.1 mmol), Ge (0.0726 g, 0.1 mmol), and Te (0.3191 g, 0.25 mmol). The mixture was loaded into a graphite crucible and transferred into a quartz tube. The tube was then evacuated to a vacuum of 10^{-3} Pa atmosphere and sealed. Afterward, the sample was heated in a resistance furnace to 1223 K over 50 h and kept at that temperature for 100 h, and subsequently cooled to 623 K at 2 K/h before switching off the furnace. Black crystals were obtained. The samples were stable in air for more than 5 months.

1.3 Second-Harmonic Generation (SHG) Measurements

The powder SHG measurements were carried out with the Kurtz-Perry method using a 2050 nm Q-switch laser.² AgGaS₂ was used as a benchmark material, which is provided by Anhui Institute of Optics and Fine Mechanics, Chinese Academy of Sciences. Ba₂Ge₂Te₅ and AgGaS₂ were ground and sieved into distinct particle size ranges (30–46, 46–74, 74–106, 106–150, 150–210 μm). The SHG signals of the frequency-doubled output emitted from the sieved samples were detected using a photomultiplier tube and recorded on the oscilloscope.

1.4 Single-Crystal Structure Characterizations

Room-temperature single-crystal XRD data were collected on an Oxford Xcalibur (Atlas Gemini ultra) diffractometer with a graphite-monochromated Mo-K α radiation ($\lambda = 0.71073$ Å). The absorption correction was done by the multi-scan method.³ The direct methods was adopted to solve the crystal structure, and refined by the full-matrix least-square fitting on F^2 using the *SHELX-2014* program package.⁴ All of the atoms were refined with anisotropic thermal parameters and a secondary extinction

Electronic Supplementary Information (ESI)

correction. Crystallographic information and selected bond distances for the title compound are summarized in Tables 1–3. CCDC number: 2094438.

2. Computational Details

The DFT calculations have been performed using the *Vienna ab initio simulation package* (VASP)^{5–7} with the Perdew-Burke-Ernzerhof (PBE)⁸ exchange correlation functional. The projected augmented wave (PAW)⁹ potentials have been used. A Γ -centered $7 \times 7 \times 7$ Monkhorst-Pack grid for the Brillouin zone sampling¹⁰ and a cutoff energy of 700 eV for the plane wave expansion were found to get convergent lattice parameters. To better describe the exchange–correlation effects of localized electrons, a hybrid functional (HSE06)¹¹ was used for the electronic structure calculations.

The imaginary part of the dielectric function due to direct inter-band transitions is given by the expression:

$$\varepsilon_2(\mathbf{h}\omega) = \frac{2e^2\pi}{\Omega\varepsilon_0} \sum_{k,v,c} \left| \langle \psi_k^c | \mathbf{u} \cdot \mathbf{r} | \psi_k^v \rangle \right|^2 \delta(E_k^c - E_k^v - E) \quad \dots\dots\dots (1)$$

where Ω , ω , u , v and c are the unit-cell volume, photon frequencies, the vector defining the polarization of the incident electric field, valence and conduction bands, respectively. The real part of the dielectric function is obtained from ε_2 by a Kramers-Kronig transformation:

$$\varepsilon_1(\omega) = 1 + \left(\frac{2}{\pi}\right) \int_0^{+\infty} d\omega' \frac{\omega'^2 \varepsilon_2(\omega')}{\omega'^2 - \omega^2} \quad \dots\dots\dots (2)$$

The refractive index $n(\omega)$ can be obtained based on ε_1 and ε_2 .

In calculation of the static $\chi^{(2)}$ coefficients, the so-called length-gauge formalism derived by Aversa and Sipe¹² and modified by Rashkeev et al¹³ is adopted, which has

Electronic Supplementary Information (ESI)

proven to be successful in calculating the second order susceptibility for semiconductors and insulators. In the static case, the imaginary part of the static second-order optical susceptibility can be expressed as:

$$\begin{aligned}
 & \chi^{abc} \\
 &= \frac{e^3}{\hbar^2 \Omega} \sum_{nml,k} \frac{r_{nm}^a (r_{ml}^b r_{ln}^c + r_{ml}^c r_{ln}^b)}{2\omega_{nm} \omega_{ml} \omega_{ln}} [\omega_n f_{ml} + \omega_m f_{ln} + \omega_l f_{nm}] \\
 &+ \frac{ie^3}{4\hbar^2 \Omega} \sum_{nm,k} \frac{f_{nm}}{\omega_{mn}^2} [r_{nm}^a (r_{mn;c}^b + r_{mn;b}^c) + r_{nm}^b (r_{mn;c}^a + r_{mn;a}^c) + r_{nm}^c (r_{mn;b}^a + r_{mn;a}^b)] \\
 & \dots\dots\dots(3)
 \end{aligned}$$

where r is the position operator, $\hbar\omega_{nm} = \hbar\omega_n - \hbar\omega_m$ is the energy difference for the bands m and n , $f_{mn} = f_m - f_n$ is the difference of the Fermi distribution functions, subscripts a , b , and c are Cartesian indices, and $r_{mn;a}^b$ is the so-called generalized derivative of the coordinate operator in k space,

$$r_{nm;a}^b = \frac{r_{nm}^a \Delta_{mn}^b + r_{nm}^b \Delta_{mn}^a}{\omega_{nm}} + \frac{i}{\omega_{nm}} \times \sum_l (\omega_{lm} r_{nl}^a r_{lm}^b - \omega_{nl} r_{nl}^b r_{lm}^a) \dots\dots\dots (4)$$

where $\Delta_{nm}^a = (p_{nn}^a - p_{mm}^a) / m$ is the difference between the electronic velocities at the bands n and m .

As the nonlinear optical coefficients is sensitive to the momentum matrix, much finer k-point grid and large amount of empty bands are required to obtain a convergent $\chi^{(2)}$ coefficient. The $\chi^{(2)}$ coefficients here were calculated from PBE wave functions and a scissor operator has been added to correct the conduction band energy (corrected to the experimental gap), which has proven to be reliable in predicting the second order susceptibility for semiconductors and insulators.

3. Figures and Tables

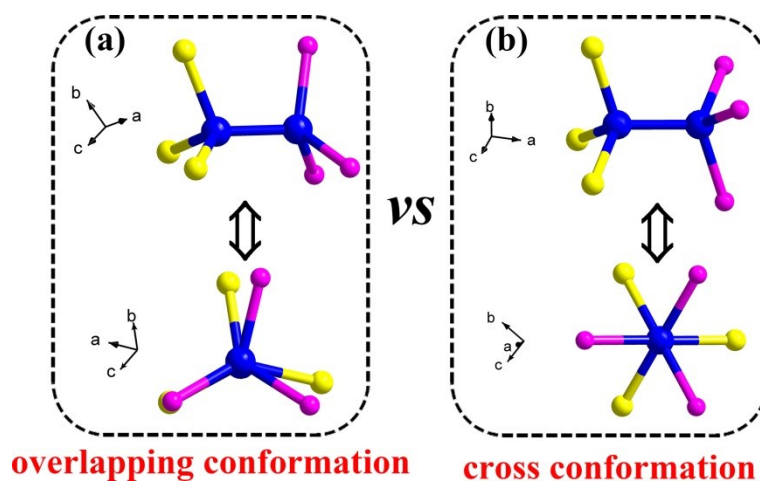


Figure S1. The ethane-like $[\text{Ge}_2\text{Te}_6]$ unit with different conformations in the Ge-based tellurides. For better expression, Te atoms on the $[\text{GeTe}_3]$ unit are represented by different colors.

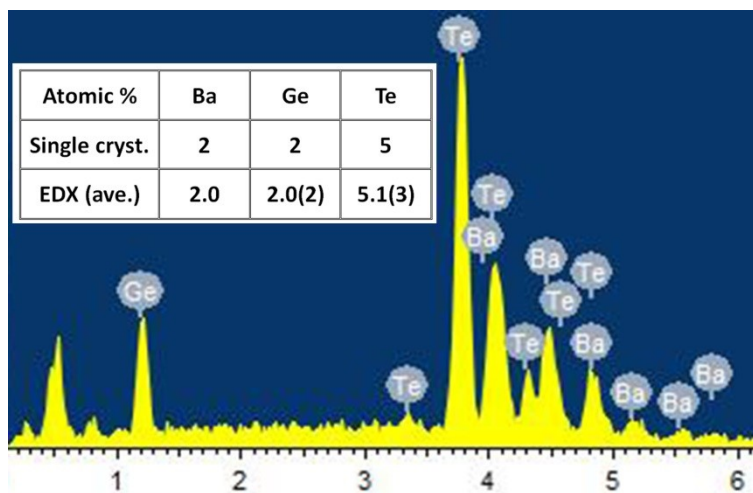


Figure S2. Energy dispersive X-ray (EDX) result and the obtained composition of $\text{Ba}_2\text{Ge}_2\text{Te}_5$.

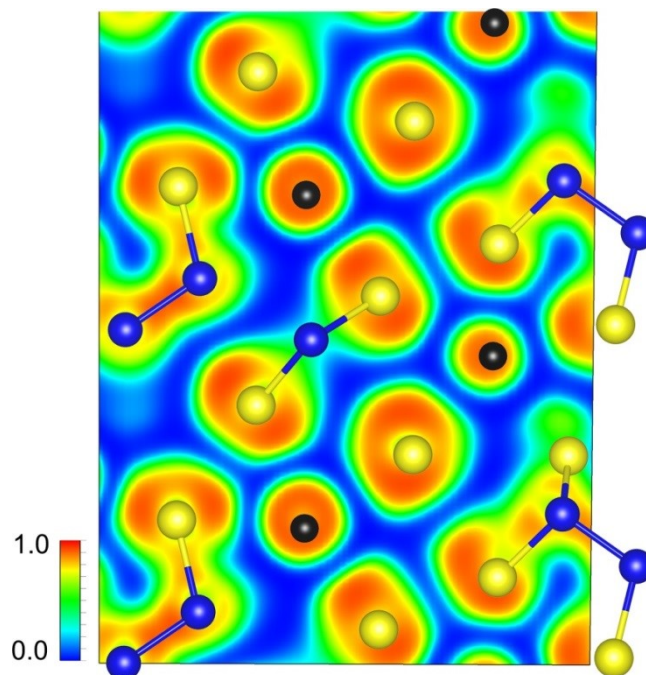


Figure S3. Electron localization function (ELF) of $\text{Ba}_2\text{Ge}_2\text{Te}_5$. Black atoms, Ba; Blue atoms, Ge; Yellow atoms, Te.

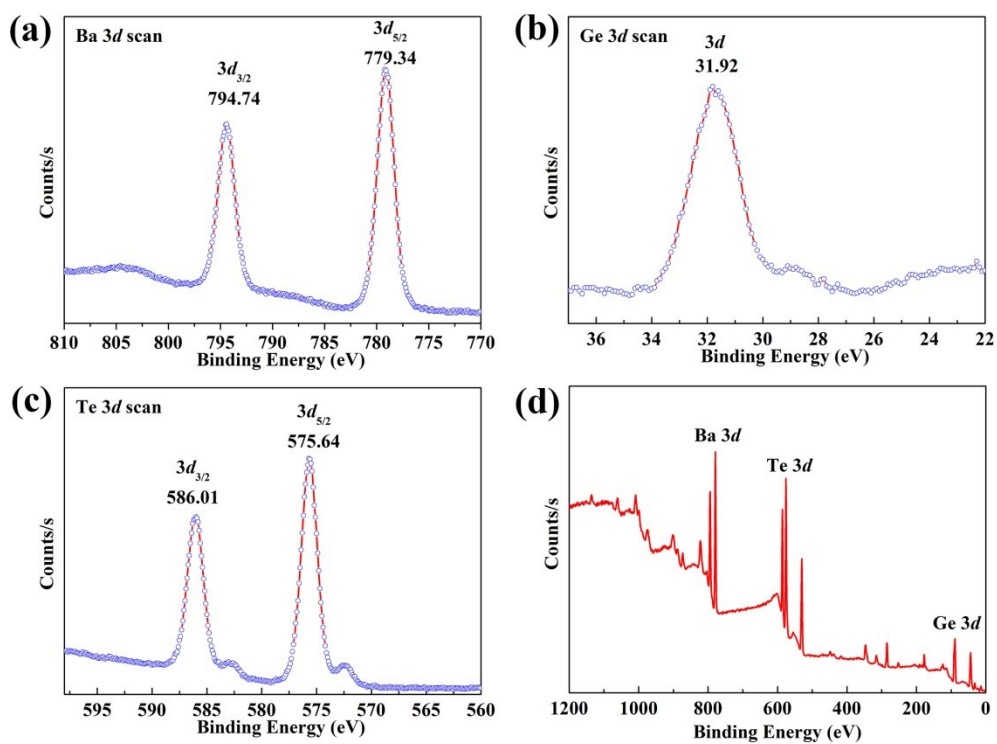


Figure S4. X-ray photoelectron spectra (XPS) of (a) Ba, (b) Ge, (c) Te, and (d) survey spectrum for $\text{Ba}_2\text{Ge}_2\text{Te}_5$.

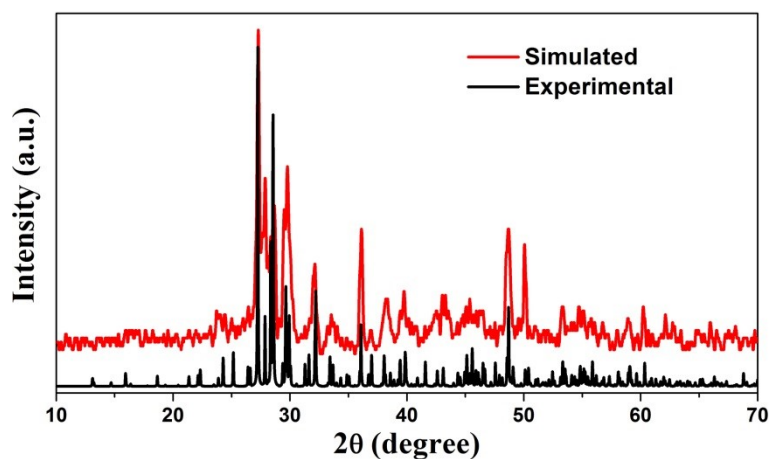


Figure S5. Powder XRD patterns of Ba₂Ge₂Te₅ heated at 1023K (red) and the simulated one (black).

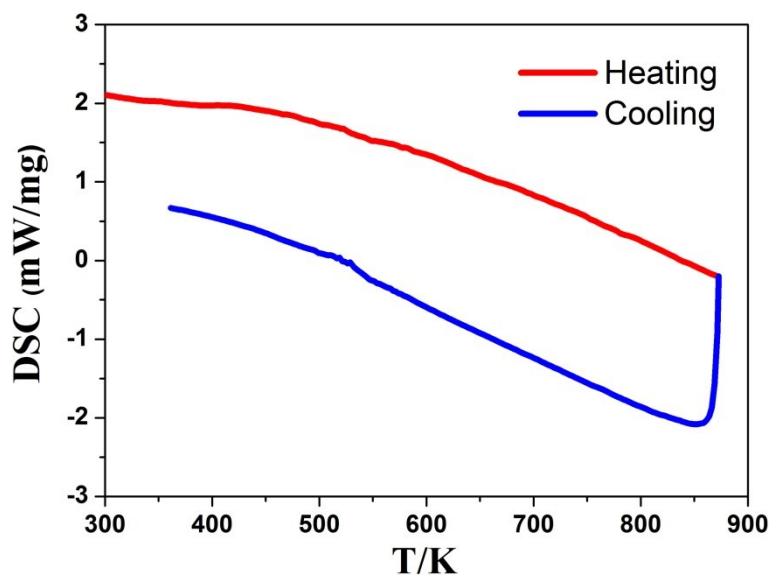


Figure S6. Cyclic DSC diagrams of Ba₂Ge₂Te₅ between room temperature and 873 K.

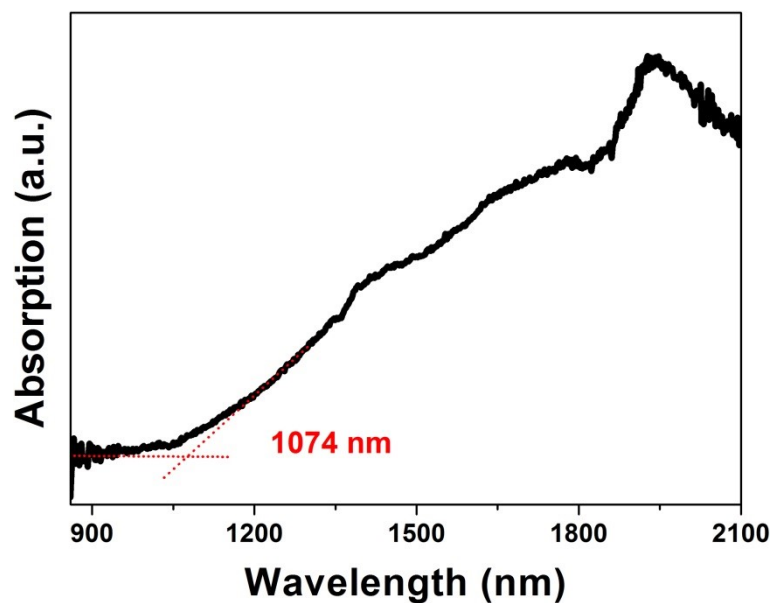


Figure S7. Vis-NIR optical absorption spectra of polycrystalline sample Ba₂Ge₂Te₅ at room temperature. The curve of Ba₂Ge₂Te₅ shows a clear absorption edge at 1074 nm, indicating a narrow band gap of about 1.15 eV.

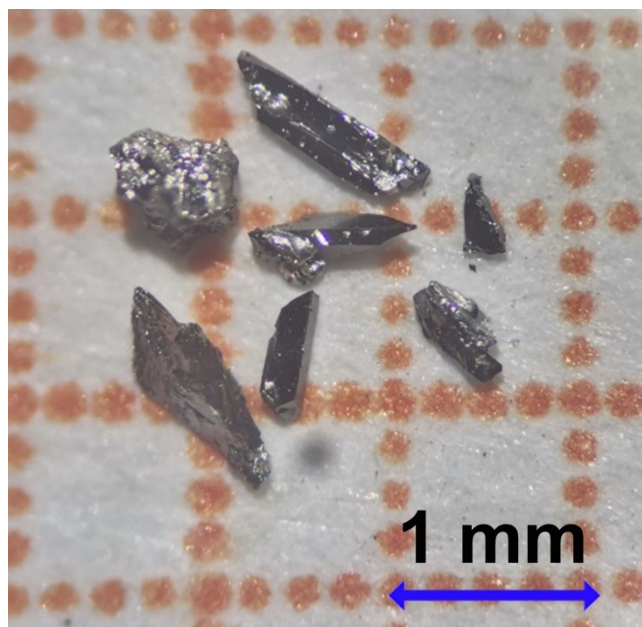


Figure S8. The photograph of single-crystal Ba₂Ge₂Te₅.

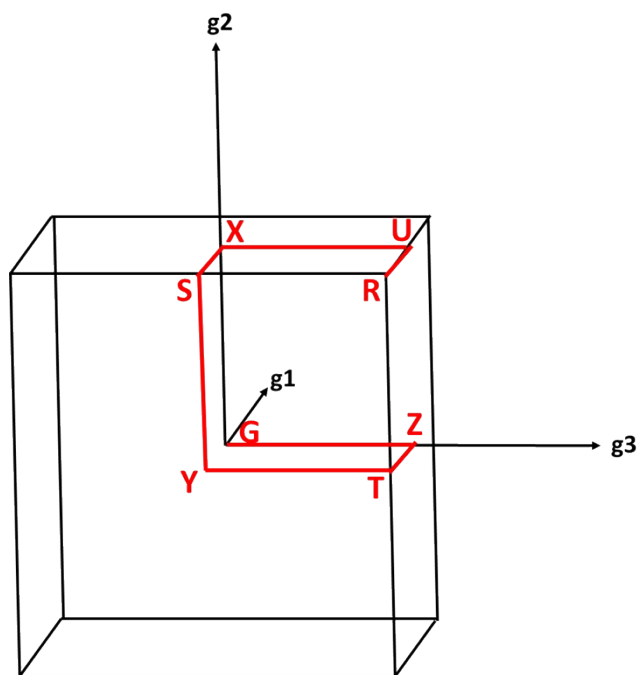


Figure S9. The first Brillouin zone with high symmetry points of Ba₂Ge₂Te₅.

Electronic Supplementary Information (ESI)

Table S1. Crystallographic data and refinement details for Ba₂Ge₂Te₅.

Empirical formula	Ba ₂ Ge ₂ Te ₅
Formula weight	1057.86
Temperature(K)	293(2)
Crystal system	Orthorhombic
Space group	<i>Pna</i> 2 ₁ (No.33)
<i>a</i> (Å)	13.393(2)
<i>b</i> (Å)	9.1769(15)
<i>c</i> (Å)	9.9500(15)
<i>V</i> (Å ³)	1222.9(3)
<i>Z</i>	4
<i>D_c</i> (g·cm ⁻³)	5.746
μ (mm ⁻¹)	22.851
GOOF on <i>F</i> ²	1.101
<i>R</i> ₁ , <i>wR</i> ₂ (<i>I</i> > 2σ(<i>I</i>)) ^a	0.0261, 0.0585
<i>R</i> ₁ , <i>wR</i> ₂ (all data)	0.0266, 0.0587
Largest diff. peak and hole (e·Å ⁻³)	1.066, -1.027

^a: $R_1 = \frac{\sum ||F_o| - |F_c||}{\sum |F_o|}$, $wR_2 = [\frac{\sum w(F_o^2 - F_c^2)^2}{\sum w(F_o^2)^2}]^{1/2}$

Electronic Supplementary Information (ESI)

Table S2. Atomic coordinates and equivalent isotropic displacement parameters of $\text{Ba}_2\text{Ge}_2\text{Te}_5$.

Atom	Wyckoff	x	y	z	$U_{\text{eq}}(\text{\AA})^a$
Ba1	$4a$	0.18113(8)	0.05958(11)	0.93736(11)	0.0144(2)
Ba1	$4a$	0.16510(8)	0.10321(11)	0.42001(11)	0.0160(3)
Ge1	$4a$	0.06346(13)	0.52365(19)	0.06408(18)	0.0119(4)
Ge2	$4a$	0.97779(14)	0.67758(18)	0.23022(18)	0.0122(4)
Te1	$4a$	0.41876(9)	0.19908(11)	0.36425(12)	0.0147(3)
Te2	$4a$	0.44453(9)	0.17790(12)	0.97219(11)	0.0150(3)
Te3	$4a$	0.28855(9)	0.87503(11)	0.65721(12)	0.0140(3)
Te4	$4a$	0.71483(9)	0.15745(11)	0.70246(11)	0.0135(3)
Te5	$4a$	0.49575(9)	0.45412(11)	0.68204(12)	0.0132(3)

U_{eq} is defined as one third of the trace of the orthogonalized U_{ij} tensor.

Electronic Supplementary Information (ESI)

Table S3. Selected bond lengths (Å) and angles (°) of Ba₂Ge₂Te₅.

Ba1–Te1	3.6419(15)	Ge1–Ge2	2.459(2)
Ba1–Te2	3.7073(16)	Ge1–Te1	2.569(2)
Ba1–Te2	3.9956(16)	Ge1–Te2	2.607(2)
Ba1–Te3	3.6511(15)	Ge1–Te3	2.578(2)
Ba1–Te3	3.5648(16)	Ge2–Te2	2.623(2)
Ba1–Te4	3.5228(15)	Ge2–Te4	2.601(2)
Ba1–Te4	3.5869(15)	Ge2–Te5	2.6069(19)
Ba1–Te5	3.5321(16)		
Ba1–Te5	3.5543(16)	∠Te1–Ge1–Te3	122.57(8)
Ba2–Te1	3.8058(16)	∠Te1–Ge1–Te2	103.28(7)
Ba2–Te1	3.5528(16)	∠Te3–Ge1–Te2	102.74(7)
Ba2–Te2	4.2019(16)	∠Ge1–Ge2–Te4	110.53(8)
Ba2–Te3	3.5621(15)	∠Ge1–Ge2–Te5	111.85(8)
Ba2–Te3	3.6668(15)	∠Te4–Ge2–Te5	100.63(7)
Ba2–Te4	3.6046(15)	∠Ge1–Ge2–Te2	115.64(9)
Ba2–Te4	3.6285(15)	∠Te4–Ge2–Te2	119.41(8)
Ba2–Te5	3.4812(15)	∠Te5–Ge2–Te2	96.53(7)
Ba2–Te5	3.4955(16)		

4. References

1. P. Kubelka, Ein beitrage zur optik der farbanstriche. *Z. Tech. Phys.*, 1931, **12**, 593–601.
2. S. K. Kurtz and T. T. Perry, A powder technique for the evaluation of nonlinear optical materials. *J. Appl. Phys.*, 1968, **39**, 3798–3813.
3. *CrystalClear* Version 1.3.5; Rigaku Corp.: Woodlands, TX, 1999.
4. G. M. Sheldrick, A short history of SHELX. *Acta Crystallogr., Sect. A: Found. Crystallogr.*, 2008, 112–122.
5. G. Kresse, VASP, 5.3.5; <http://cms.mpi.univie.ac.at/vasp/vasp/vasp.html>.
6. G. Kresse and J. Furthmuller, Efficient iterative schemes for ab initio total-energy calculations using a plane-wave basis set. *Phys. Rev. B: Condens. Matter*, 1996, 11169–11186.
7. G. Kresse and D. Joubert, From ultrasoft pseudopotentials to the projector augmented-wave method. *Phys. Rev. B: Condens. Matter*, 1999, **59**, 1758–1775.
8. P. E. Blochl, Projector augmented-wave method. *Phys. Rev. B: Condens. Matter*, 1994, **50**, 17953–17979.
9. J. P. Perdew, K. Burke and M. Ernzerhof, Generalized Gradient Approximation Made Simple. *Phys. Rev. Lett.*, 1996, **77**, 3865–3868.
10. D. J. Chadi, Special points for Brillouin-zone integrations. *Phys. Rev. B: Condens. Matter*, 1976, **16**, 1746–1747.
11. J. Heyd, G. E. Scuseria and M. Ernzerhof, Hybrid functionals based on a screened Coulomb potential. *J. Chem. Phys.*, 2003, **118**, 8207–8215.

Electronic Supplementary Information (ESI)

12. C. Aversa and J. E. Sipe, Nonlinear optical susceptibilities of semiconductors: Results with a length-gauge analysis. *Phys. Rev. B*, 1995, **52**, 14636–14645.
13. S. N. Rashkeev, W. R. L. Lambrecht and B. Segall, Efficient ab initio method for the calculation of frequency-dependent second-order optical response in semiconductors. *Phys. Rev. B*, 1998, **57**, 3905–3919.